Tailoring Electromagnetic Responses in Terahertz Metasurface by Breaking the Structural Symmetry in T-Shaped Resonators

Changxiang Liu, Dongsheng Li, Philippe Boutinaud, Jie Xu, Yongping Du, Yidong Hou, Cunlin Zhang, Qingli Zhou,* and Fengwen Kang*

Herein, the design of terahertz metasurface with symmetric T-shaped resonators and the corresponding bright and dark modes are reported on. It is demonstrated that the dark mode evoked by breaking the structural symmetry is insensitive to the X-polarized electric field and a typical electromagnetically induced transparency (EIT) effect is also observed in the numerical simulation when introducing a relatively low structural asymmetry where the dark and bright modes are modified to the same frequency. To explain the underlying mechanism, theoretical calculations based on the coupled Lorentz oscillator model are performed. In terms of the desirable fittings with the simulation results, it is confirmed that there exists the dark mode in the symmetric T-shaped resonators and the coupling between the bright and dark modes enhanced by the structural–symmetry breaking is responsible for the observed EIT effect. It is shown in the results further that the structural asymmetry degree has close relation with the coupling strength resonance and can thereby greatly affect the oscillation resonance splitting in frequency that it is reflected by the change of the bandwidth of the transparency window. In addition, the experimental spectra showing the characteristic of broadband transparency window are explained by the excitation of the dark mode whose frequency deviates from the bright mode.

1. Introduction

Electromagnetically induced transparency (EIT) is known to be a coherent optical nonlinearity that renders a medium transparent within a narrow spectral range around an absorption line.[1,2] As early stated by Liu et al.[3] and reviewed by other followers or works,[1,2,4] EIT in essence is a destructive quantum interference phenomenon of bright–dark mode coupling between two excited pathways in a three-level atomic system that results in a sharp transparency peak at a specific frequency in the transmission spectrum and that can thereby permit the propagation of light through an otherwise opaque atomic medium. So far, EIT has been reported in many systems including hybrid metallic nanoparticle–quantum dot hybrid systems;[5] superconducting niobium nitride (NbN) films;[6] quasi-1D gases in which the atoms interact via exchange interactions;[7] single atoms quasi-permanently trapped inside a high-finesse optical cavity;[8] plasmonic metasurfaces consisting of Au nanobars arranged in pi, H, and four-shaped fashion;[9] whispering-gallery-mode microresonators in the

C. Liu, D. Li, F. Kang
College of Materials Science and Engineering
Sichuan University
Yihuan Road No. 24 South Section 1, Chengdu, Sichuan 610065,
P. R. China
E-mail: kangfengwen0597@126.com

C. Liu, C. Zhang, Q. Zhou
Key Laboratory of Terahertz Optoelectronics
Ministry of Education, and Beijing Advanced Innovation Center for
Imaging Theory and Technology
Department of Physics
Capital Normal University
Beijing 100048, P. R. China
E-mail: qlzhou@cnu.edu.cn

P. Boutinaud
Clermont Auvergne INP
CNRS
ICCF
Université Clermont Auvergne
F-63000 Clermont-Ferrand, France

J. Xu
School of Medical Information and Engineering
Southwest Medical University
Luzhou 646000, P. R. China

Y. Du
MIIT Key Laboratory of Semiconductor Microstructure and Quantum
Sensing
Department of Applied Physics and Institution of Energy and
Microstructure
Nanjing University of Science and Technology (NUST)
Nanjing, Jiangsu 210094, P. R. China

Y. Hou
College of Physics
Sichuan University
Yihuan Road No. 24 South Section 1, Chengdu, Sichuan 610065,
P. R. China

**ADVANCED
SCIENCE NEWS**

www.advancedsciencenews.com

**ADVANCED
PHOTONICS
RESEARCH**
Open Access

www.adpr-journal.com

coupled fused-silica microspheres;[10] and/or others like quantum optomechanical systems.[11] In addition, the EIT effect has also involved (but is not limited to) 1) in the enhancement of the nonlinear optical behavior of the plasmon-integrated photonic or communication systems;[12,13] 2) in the improvement of the optical sensing performance of plasmonic structure consisting of three bars; among that, two of bars are parallel to each other but perpendicular to the third bar;[14] 3) in slowing down the propagation of light in periodic 2D structures,[15,16] etc.

However, sustaining the coherency of the excitation pathways in atomic systems/levels during propagation usually requires stringent experimental conditions like cryogenic temperature[17,18] or high-intensity laser beam as incoming light.[19,20] As a result, this, together with the limited number of reported EIT-related materials at present, greatly limits "in-depth" study on the EIT effect, particularly when associated with practical applications. The difficulty to some extent can be resolved by designing metasurfaces that can mimic the behavior of the electromagnetic waves involving the EIT effect. It should be noted that the metasurfaces, typically for those composed of a periodic array of sub-wavelength, are also often relevant to achieve the intriguing electromagnetic transparency window taking place in the terahertz (THz) spectral region through destructive interference of surface plasmons inside artificial meta-molecule.[21,22] This therefore means that the EIT-related quantum effect can be classically mimicked in THz metamaterials.

In most cases, the EIT effect can be realized in the THz metasurface via a bright–dark-coupling scheme[23,24] where the resonances of the bright and dark modes usually share a nearly identical frequency with different Q-factors. However, there are also some typical exceptions[25,26] that they involve a bright–bright-coupling scheme based on two hybridized bright modes (e.g., placed in close proximity to another), the detuning frequency of which enables the EIT effect. In addition, some archival literature[27–29] also report that the EIT effect can be aroused by breaking and/or manipulating the symmetric structure of the unit cell in the THz metasurface, but most of them just show the symmetry-breaking-related EIT phenomenon, without discussing and/or analyzing the mechanistic origin from a theoretical viewpoint. Exemplarily reported by Chowdhury et al. in ref. [29], the authors used the perturbation theory to explain how the dark mode is excited in the symmetry-broken THz metamaterials, but a more reliable theoretical calculation is lacking.

In light of the previous analysis, here, we designed the THz metasurface with symmetric T-shaped resonators and studied the corresponding bright and dark modes. In our design, we treated the unit cell of T-shaped resonator as a whole to study the structural symmetry-breaking-induced EIT effect in THz metasurface with T-shaped resonators and the optical behaviors of the broadband transparency window. This design consideration differs from most of recent reports which studied the EIT effect by, for instance, separating the unit cell into two or more individual parts[30–33] to serve as the bright and dark modes,

respectively. The T-shaped resonators proposed in our work cover the advantages of the following: 1) they feature simple structures but desirable phenomenon, which definitely is good for mechanism study; 2) the bright and dark modes of the T-shaped resonators are simple, corresponding to the oscillation excited with X- and Y-polarized THz wave, respectively, thus it can allow easy measurement or characterization for both bright and dark modes; 3) the bright and dark modes, as we will show in Figure 3, feature dipole resonance with a lower Q factor and double inductive-capacitive-like (DLC) resonance with a higher Q factor, respectively, which is conducive to the excitation of the EIT effect. Specifically, doing so, here, we discovered that the bright and dark modes, the resonances of which were excited respectively by X- and Y-polarized electric fields, coexist in the designed T-shaped resonator. By use of the coupled Lorentz oscillator model to theoretically fit into the simulated EIT effect, we showed that the dark mode is indirectly excited by the bright mode due to the structural symmetry breaking. Additionally, we revealed further that this evoked dark mode can act back on the bright mode, causing a strong destructive interference that results in the EIT effect. Meanwhile, the symmetry-breaking-evoked dark mode, which was found to depart from the bright mode in frequency, can nicely explain why the symmetry-breaking-mediated resonance appears at the lower/higher frequency in the experiment. Therefore, we conclude that this dark and bright modes' interplay plays a key role in forming the observed broadband transparency window. Based on the insights into the symmetry-breaking-induced EIT effect, the present report presents feasible strategy or design consideration for achieving asymmetric planar metasurfaces with controllable EIT and broadband transparency characteristics. In this situation, such metasurfaces may be potentially applied in, for example, biological sensing and molecule detection,[34,35] THz sensing,[36] or optical communication technology.[37–39] Obviously, this work not only reports the resonant modes in the symmetry-broken THz metasurface but also provides some insights into understanding the symmetric-breaking-induced EIT effect.

2. Design and Experimental Details

2.1. Consideration on the Design of T-Shaped Resonator

In our metasurface unit cell (**Figure 1**a), a symmetric T-shaped resonator formed by connecting a gold (Au) vertical cut wire (VCW) to an Au horizontal cut wire (HCW) is designed to metallize on a high-resistivity silicon substrate of 500 nm in thickness (t). The length (l) and width (w) of both VCW and HCW in each T-shaped resonator are $l = 36\,\mu m$ and $w = 6\,\mu m$, respectively. Note that the thickness the metalized Au layers is fixed as 200 nm. The size of a period (P) for each square unit cell is 60 μm. The unit cell with structural symmetry breaking, as seen in Figure 1b, is designed by horizontally moving the VCW along axis x where the displacement distance (S), relative to the vertical symmetry axis of HCW, is varied from 0 to 15 μm. With the preconceived T-shaped structures, we manufactured the metasurfaces using a photolithography method followed by a thermal evaporation route.[40,41] Figure 1c shows the corresponding optical microscopic images locally containing a 2D periodicity of

F. Kang
Laboratory of Advanced Nano Materials and Devices
Institute of Materials Technology (IMT)
Ningbo Institute of Materials Technology and Engineering (NIMTE)
Chinese Academy of Sciences (CAS)
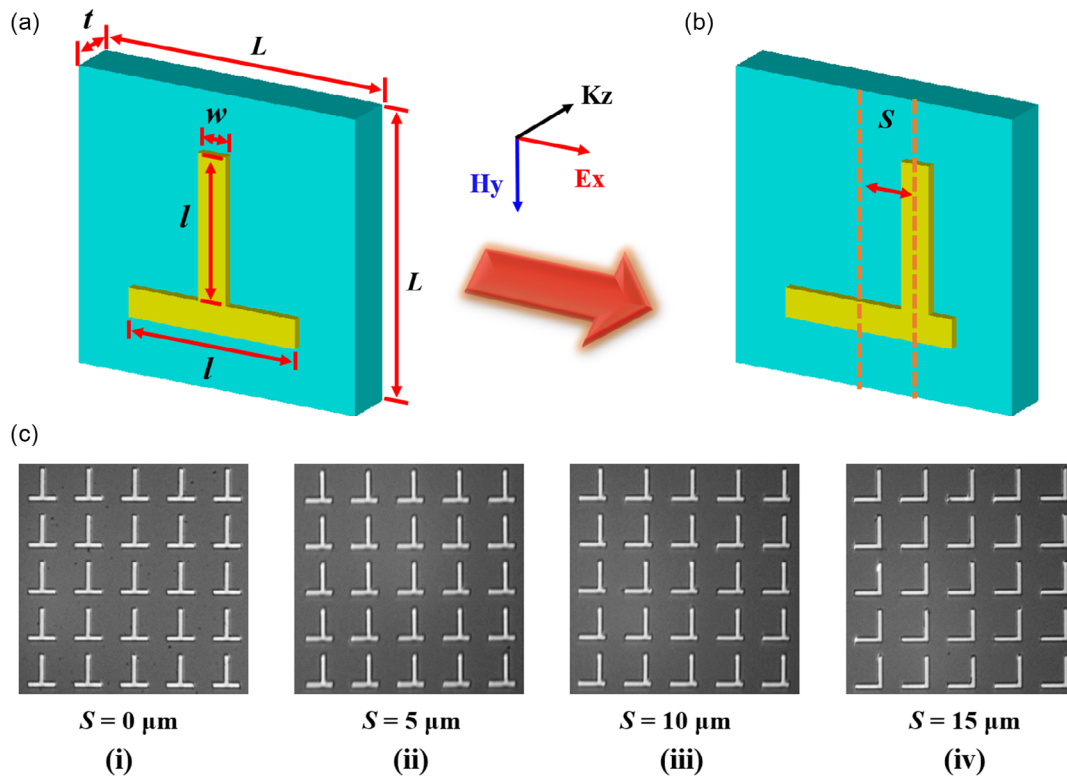Ningbo 315201, P. R. China

Figure 1. a) Schematic of the symmetric T-shaped resonator in a unit cell, and b) that of moving the vertical cut wire (VCW) horizontally with a displacement distance (S). c) Optical microscopic images of the microstructural samples with the S values of i) 0, ii) 5, iii) 10, and iv) 15 μm, respectively. Note that in this figure, the geometric parameters are $l = 36$ μm, $w = 6$ μm, $L = 60$ μm, and $t = 500$ nm, respectively; Kz, Ex, and Hy denote the terahertz (THz) wave number, electric-field intensity, and magnetic-field intensity propagated along axis z, x, and y, respectively.

5×5 unit cells (i.e., $P = 25$ μm) with the S values of i) 0, ii) 5, iii) 10, and iv) 15 μm.

2.2. Spectroscopic Measurements

The manufactured microstructures containing the T-shaped resonators are vertically illuminated with a THz beam propagating along the vertical y-axis direction with an electric field (E) oriented along the horizontal x-axis direction. In parallel, a bare silicon substrate was also used here as a reference to normalize the transmission spectra in the frequency domain. The spectroscopic measurements were collected on a THz time–domain spectroscopic system that was equipped with an 800 nm 80 MHz femtosecond (fs) laser to generate the THz source. When the photoconductive antenna was irradiated by the fs laser, the THz-pulsed signals with width of several picoseconds were generated and, with the help of the photoconductive antenna detection, could be converted into frequency spectra having ≈2.5 THz in width. The whole testing process was performed in a gaseous N_2 environment.

2.3. Theoretical Details on the Simulation Method

Numerical simulations implemented with the finite-difference time-domain (FDTD) algorithm were performed to study the underlying mechanism responsible for our experimental spectra.

Owing to its high resistivity, the used silicon substrate was assumed as a nondispersive material featuring low absorption in the THz frequency region. It was modeled here as a lossless dielectric with $\varepsilon = 11.78$.[42] Since the grain boundaries and defects can bring about additional scattering,[43] the dispersion relation of the electromagnetic wave, which is otherwise suitable for modeling the dispersion characteristics of bulk metals like gold (Au), silver (Ag), and aluminum (Al) at THz frequency region,[44] becomes inapplicable to the ultrathin metallic films. In this situation, the Au metal with a direct-current (DC) conductivity of 4.6×10^7 S m^{-1} at room temperature was used in our simulation.

3. Results and Discussion

3.1. Observation on EIT Effect and Theoretical Simulation

In **Figure 2**, graphs (b) and (e) show the transmission spectra where we have chosen the displacement distance for four S values and for two orientations (i.e., 0° and 90°, as pictured in graphs (a) and (d)) of the metasurfaces with respect to the incoming electric field. Each spectrum corresponding respectively to graphs (b) and (e) is simulated in graphs (c) and (f). Considering first the case of the 0° configuration that corresponds to graph (a) and the related graphs (b) and (c), we can note that when $S = 0$ (i.e., symmetric T-shaped resonators), only one high-frequency resonance (ν_h) band appears at ≈1.39 THz.
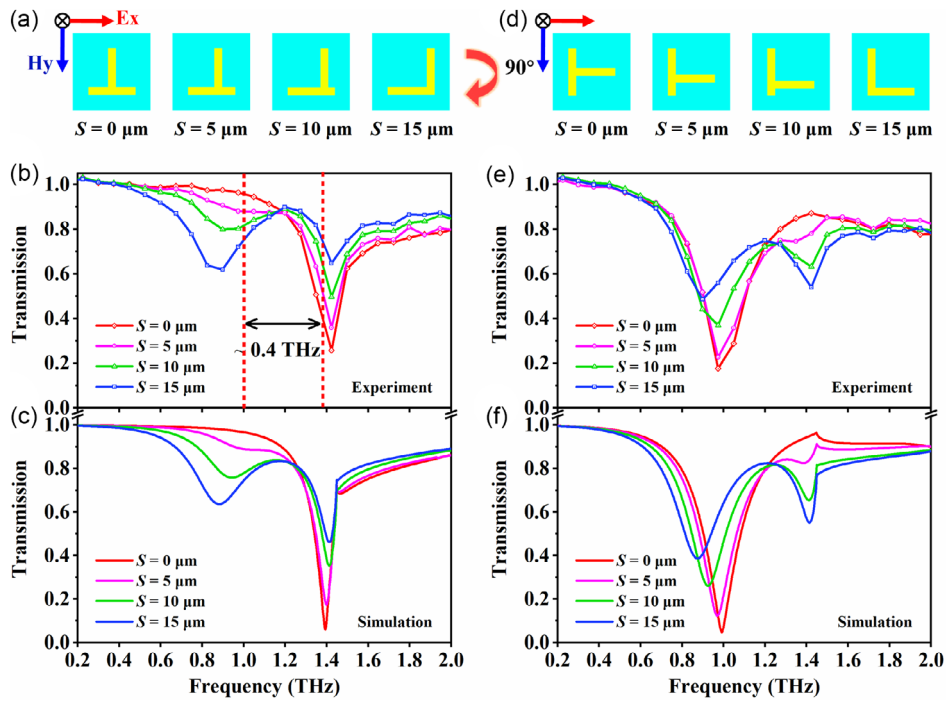
Figure 2. a) Schematic diagram of the T-shaped resonators by moving the VCW horizontally with a displacement distance (S) of 0, 5, 10, and 15 μm. b) Experimental and c) simulated transmission spectra of the samples pertaining to S = 0, 5, 10, and 15 μm, respectively. d) Schematic diagram of the T-shaped resonators and e) the corresponding experimental and f) simulated transmission spectra for S = 0, 5, 10, and 15 μm after rotation by 90° clockwise.
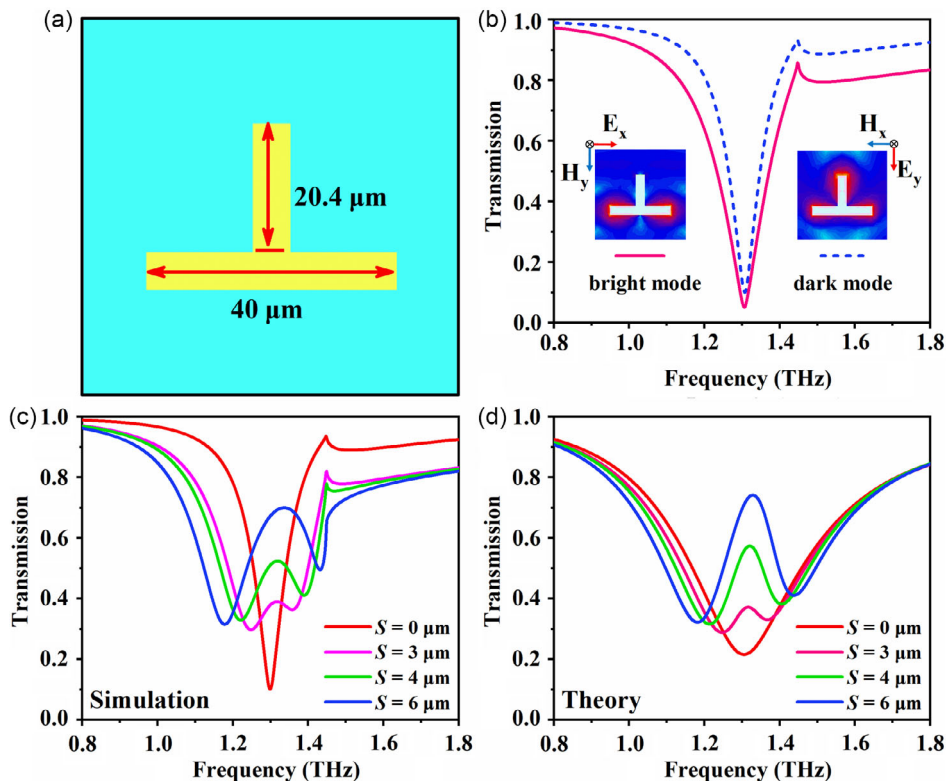

Figure 3. a) Schematic diagram of the modified unit cell, among which the horizontal cut wire (HCW) and VCW of the T-shaped resonator are set to be 40 and 20.4 μm, respectively. b) Simulated transmission spectra of the modified symmetric T-shaped structure upon excitation with X- (red real line) and with Y- (blue dash line) polarized THz wave. c) Simulated and d) theoretical calculated transmission spectra for S = 0, 3, 4, and 6 μm, respectively.

**ADVANCED
SCIENCE NEWS**

www.advancedsciencenews.com

**ADVANCED
PHOTONICS
RESEARCH**
Open Access

www.adpr-journal.com

However, breaking the structural symmetry, as depicted in graphs (e) and (f), results in a low-frequency resonance (v_l) that experiences a gradual decrease in the absorption intensity at the expense of the ≈1.39 THz resonance as S is increased from 0 to 15 μm, concomitantly with a slight blueshift in frequency from 1.0 to 0.87 THz. In contrast, the high-frequency resonance, measured over the same increment range of the displacement S values, shows a gradual decrease in the absorption intensity and a slight redshift in frequency. Typically, a transparent window, with a spectral bandwidth of up to ≈0.4 THz for $S = 15$ μm, as seen in graph (b), is generated in the experiment. Importantly, the related experimental data are nicely simulated and agree well with the simulated curves (see graph (c)), although a simulated redshift of the 1.39 THz resonance (graph (c)) is slightly more pronounced than that experimentally observed in graph (b) as the S value is raised. Moreover, the simulated low-frequency resonance band at, for instance, ≈1.0 THz for $S = 5$ μm, is clearer as compared to the counterpart that we experimentally observed. A step further, when the as-manufactured samples were rotated 90° clockwise (Figure 2d) and then submitted to the same experimental conditions, the transmission spectra (see Figure 2e) also contain high- and low-frequency resonance bands, but a mirror-image behavior appears. A gradual increase of the absorption intensity along with a slight redshift of the position in frequency is observed in the high-frequency resonance (v_h) as the S value is raised from 0 to 15 μm. At the same time, the low-frequency resonance band upon the same change of the S value undergoes an inverse shift in frequency from 0.87 to 1 THz and a gradual decrease of its absorption intensity. As expected, the mirror-image behaviors in the experiment can be reproduced well by the simulation based on the FDTD computational method (Figure 2f). These two analyzed configurations vividly confirm the formation of a transparency window with a spectral bandwidth of up to ≈0.4 THz as revealed by the typical spectral curve of $S = 15$ μm in Figure 2b.

As a matter of fact, our original motivation in designing the THz metasurfaces in T-shaped resonators (Figure 1) was to allow VCWs and HCWs with identical length and width to serve respectively as the bright and dark modes, so as to obtain the transparency window and reveal the relevant spectral characteristics by use of an EIT-related theory based on the bright-dark-coupling scheme. The experimental and simulated spectra, as seen in Figure 2, however, are inconsistent with our initial expectations. First of all, these spectra fail to comply with the EIT characteristics strictly, since there is neither obvious transformation of the resonance dip into the transmission peak nor resonance splitting near the resonance dip. Second, the underlying reasons why there are the resonances at 1.0/1.39 THz and why they just appear at 1.0/1.39 THz once the structural symmetry in the T-shaped resonator is broken are still an unresolved issue. In this case, to go deeper into these aspects, unlike the T-shaped structure whose united cell is simply consisted of individual HCW and VCW with the same horizontal and vertical lengths, we here simulate the transmission spectra by changing the lengths of the VCW (i.e., $l = 20.4$ μm) and HCW (i.e., $l = 40$ μm) bars but retain 6 μm for their widths. Within this new configuration (see **Figure 3**a), the resonances excited with X- or with Y-polarized THz wave are found to share the same frequency at 1.305 THz. The corresponding experimental spectrum is shown in Figure 3b. Interestingly, we found that the T-shaped

resonator excited with the horizontal and vertical E fields features a broadband dipole resonance with a lower Q factor and a DLC resonance with a higher Q factor, respectively. In this case, by considering the EIT theory based on the bright-dark-coupling scheme, a hypothesis, involved that the bright and dark modes in this T-shaped resonator are excited by X- and Y-polarized electric fields, respectively, is proposed in this present work. That is, the structural symmetric breaking in the T-shaped resonator can, on the one hand, induce the dark mode excitation and, on the other hand, the destructive coherent interference between the bright and dark modes brings about the EIT effect. In the configuration depicted in Figure 3a, the displacement distance S that breaks the symmetry of the T-shaped resonator is defined to be 0. Simulations (Figure 3c) and calculations (Figure 3d) of the transmission spectra were achieved by varying the S from 0 to 6 μm. It is obvious that the variation trend basically matches with each other. In this situation, a typical structural symmetry-breaking-induced EIT effect, accompanied with a gradual transformation of the fundamental resonance dip (≈1.305 THz) into the transparent peak and a significant resonance splitting, is observed. However, one obvious difference is that the calculated resonance and its related transmissivity at $S = 0$ μm, as seen in Figure 3c,d, is broader and higher when compared respectively to the corresponding simulated resonance. Additionally, there is another obvious difference that the simulated transmissivity is lower than the calculated transmissivity when the frequency spectrum is either less than 1.0 THz or greater than 1.6 THz. Meanwhile, the transmissivity of the low-frequency resonance in the simulated spectrum for $S = 6$ μm is lower than that in the simulated spectrum for $S = 4$ μm; whereas the transmissivity of the low-frequency resonance in the calculated transmission spectrum for $S = 6$ μm is almost the same as that in the simulated transmission spectrum for $S = 4$ μm. To further illustrate the simulated EIT results shown in Figure 3c, the T-shaped resonators, with the VCW bars of 18.5 and 22.55 μm yet the corresponding HCW bars of 36 and 44 μm, are also simulated, as depicted in **Figure 4**a,d, respectively. The simulated frequency spectra of bright and dark modes have the same oscillation frequency (Figure 4b,e), and they still can exhibit the typical EIT effect when the structural symmetry is broken (Figure 4c,f).

To better understand the nature of the simulated resonances, we also studied the distribution of the displacement distance (S)–dependent surface current and electric field at resonances of these T-shaped resonators. The results are shown in **Figure 5**. For the symmetric structure, the electric field is confined to the two ends of the HCW bar (Figure 5a), showing its role in driving the current oscillation in HCW. The current oscillation features a broad dipole resonance with a relatively low Q factor due to the strong scattering. Once the structural symmetry is broken, the dipole resonance splits into two dips, as exemplarily illustrated by resonances v_l and v_h marked in Figure 5b(i, v) for $S = 6$ μm. The current- and electric-field distributions pertaining to $v_l = 1.18$ THz and $v_h = 1.43$ THz, as respectively marked by arrows in Figure 5b(ii, ii) and (v, vi), reveal that most of the current oscillation is distributed into the left and right sides of the asymmetric T-shaped resonator. Since there is a phase difference between the current oscillation of dark and bright modes, the current distribution generated with static v_l and v_h excitation can be illustrated in terms of the current superposition of the bright and dark modes (Figure 5c). Moreover, the
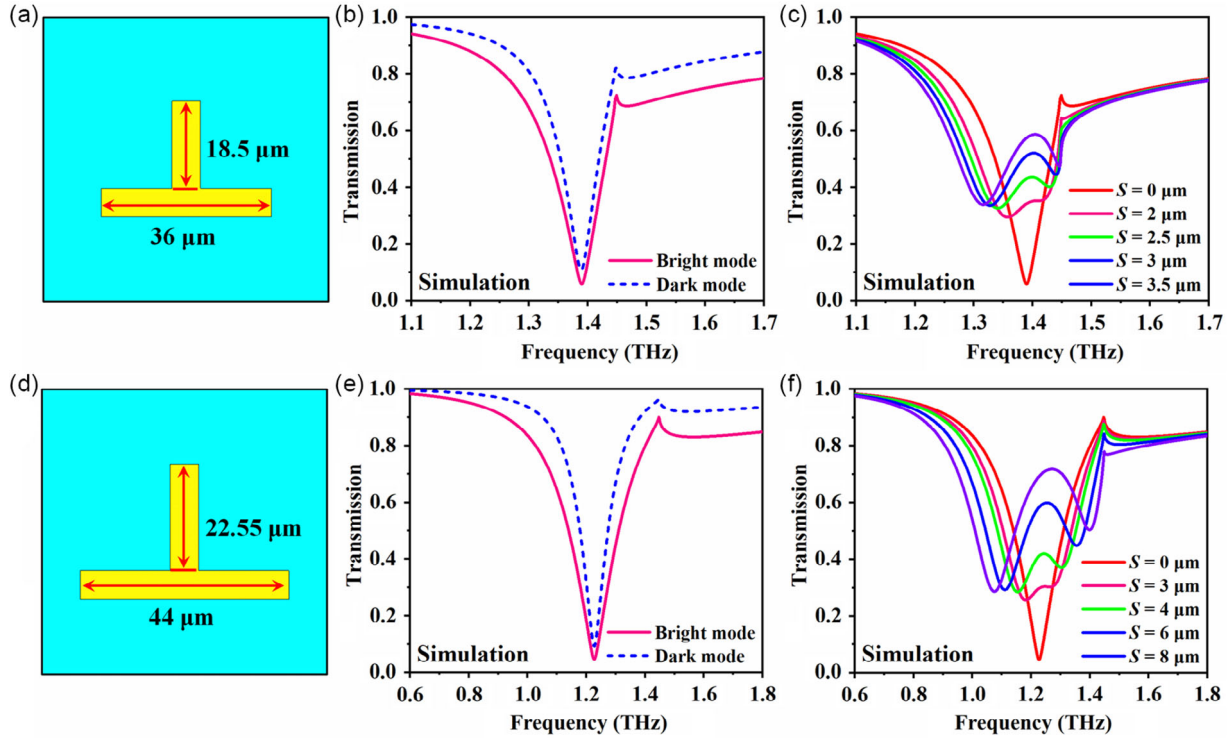
Figure 4. a) Schematic diagram of the T-shaped resonators with the HCW bar of 36 μm and VCW bar of 18.5 μm, and b) relevant simulated bright and dark modes, and c) transmission spectra with the S values of 0, 2, 2.5, 3, and 3.5 μm. d) Schematic diagram of the T-shaped resonators with the HCW bar of 44 μm and VCW bar of 22.55 μm, and e) relevant simulated bright and dark modes, and f) transmission spectra with the S values of 0, 3, 4, 6, and 8 μm.

v_l and v_h resonance frequencies depend strongly on the oscillation length of the driven currents. Typically, the electric-field distribution of the transparency peak resonance (v_t) at 1.305 THz (Figure 5b(iv)) is analogous to the dark mode resonance, indicating that the dark mode is indirectly driven by the symmetric breaking. However, there is coherent destructive interference between the excitation of bright and dark modes, which can in turn largely suppress the current oscillation of HCW and thereby allows the incident wave to be transmitted.

3.2. Mechanistic Analysis and Interpretation

To understand why the T-shaped resonator features the EIT effect when its symmetric structure is broken, the coupled Lorentz oscillator theory was implemented in our simulation procedure of the transmission spectra depicted in Figure 3c. Accordingly, the coupled system was first treated as two damped harmonic oscillators with Equations (1) and (2)[23,45]

$$\ddot{x}_1 + \gamma_1 \dot{x}_1 + \omega_1^2 x_1 + \kappa x_2 = gE \tag{1}$$

$$\ddot{x}_2 + \gamma_2 \dot{x}_2 + \omega_2^2 x_2 + \kappa x_1 = 0 \tag{2}$$

where the Equations (1) and (2) pertain to the bright and dark modes, respectively, and they are used here for modeling the oscillators that are driven by the external electric field E and that do not interact with the external given electric field. The quantities (ω_1, ω_2), (x_1, x_2), and (γ_1, γ_2) represent the circular

frequencies, amplitudes, and damping rates of the bright and dark modes, respectively. κ denotes the coupling coefficient between the bright and dark modes, and g accounts for the strength by which the bright mode couples to the incident THz laser E field. Note that the dark mode that is indirectly excited by the near field coupling to the bright mode is also modeled by Equation (2). With Equations (1) and (2), the oscillation amplitude of the bright and dark modes can be formulated following

$$x_1(\omega) = \frac{\omega_2 - \omega + i\gamma_2\omega}{(\omega_1^2 - \omega^2 + i\gamma_1\omega)(\omega_2^2 - \omega^2 + i\gamma_2\omega) - \kappa^2} gE \tag{3}$$

$$x_2(\omega) = -\frac{\kappa}{(\omega_1^2 - \omega^2 + i\gamma_1\omega)(\omega_2^2 - \omega^2 + i\gamma_2\omega) - \kappa^2} gE \tag{4}$$

As indicated in the refs. [23,45,46], the susceptibility of a metal structure layer with a thickness of d can be expressed by

$$\chi = \frac{P}{\epsilon_0 Ed} \propto \frac{x_1}{Ed} \tag{5}$$

Taking into consideration the Fabry–Perot interference occurring in the THz wave propagating in a ultrathin metal structure layer, we express the transmission $t_M(\omega)$ of our T-shaped metal structure layer as

$$t_M(\omega) = \frac{4n_V n_M e^{i\frac{\omega}{c}n_M d}}{(n_V + n_M)(n_M + n_S) - (n_M - n_S)(n_M - n_V)e^{i\frac{\omega}{c}2n_M d}} \tag{6}$$

where n_V, n_M, and n_S are the refractive indexes of the vacuum, metal structure layer, and substrate, respectively. c is the light
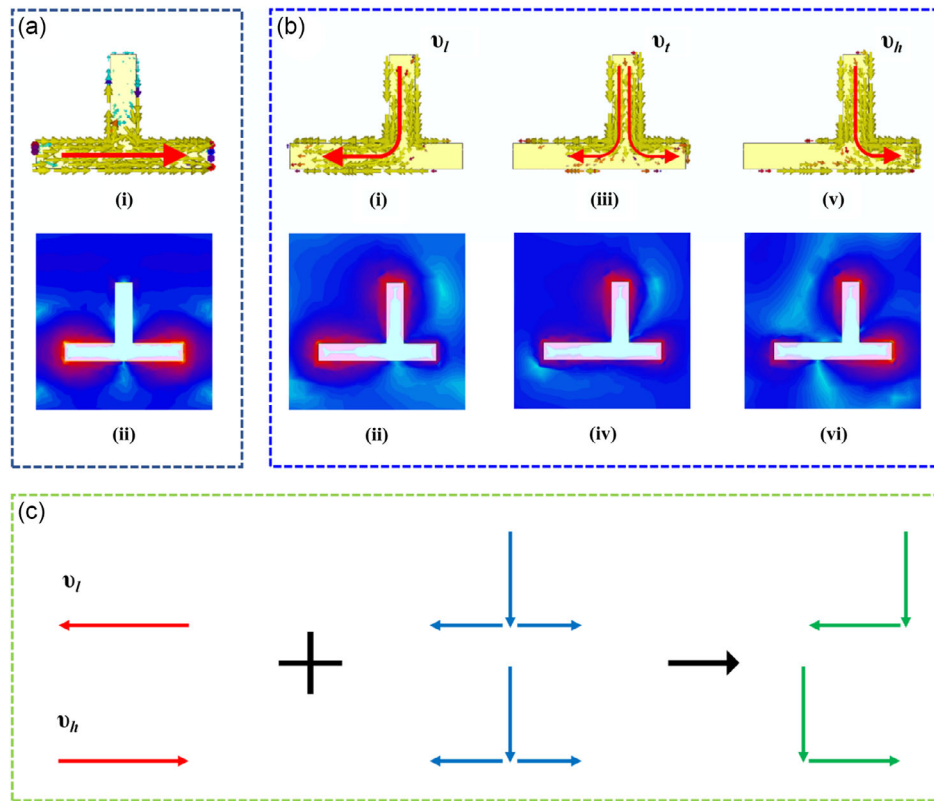
Figure 5. a) i) Surface currents and ii) electric-field distributions at 1.305 THz for the symmetric structure with $S = 0\,\mu m$. b) i, iii, v) Surface currents and ii, iv, vi) electric-field distributions at i, ii) v_l, iii, iv) v_t, v, vi) v_h for $S = 6\,\mu m$, respectively. c) Schematic diagram illustrating the static current superposition of the bright and dark modes at v_l and v_h.

celerity in vacuum. The vacuum–substrate interface transmission $t_R(\omega)$ that we used as a reference for the normalization of the transmission spectra obeys

$$t_R(\omega) = \frac{2n_V}{n_V + n_S} \tag{7}$$

By combining Equations (6) and (7), we can finally express the transmission of the T-shaped metal structure layer as

$$t(\omega) = \lim_{d \to 0} \left| \frac{t_M(\omega)}{t_R(\omega)} \right|^{d \to 0} \Rightarrow \left| \frac{c(1 + n_{sap})}{c(1 + n_{sap}) - i\omega d\chi} \right| \tag{8}$$

As a result, the S-dependent transmission spectra pertaining to the structure depicted in Figure 2 can be simulated, which, as depicted in Figure 3c, agree well with the fitted transmission spectra shown in Figure 3d. The fitted parameters γ_1, γ_2, κ, δ_1, and δ_2 against displacement distance (S), which are obtained by fitting into the intensity fluctuation and frequency shift, are listed in **Table 1**. Their dependence with S value is reproduced in **Figure 6**a,b.

As the displacement S value increases from 0 to $6\,\mu m$, the damping rates γ_1 and γ_2 can retain constant (i.e., 0.75 and 0.69 rad ps^{-1}, respectively) while the coupling coefficient κ increases from 0 to 11.94 rad^2 s^{-2}. Additionally, in terms of the bright and dark modes lying in the same T-shaped resonator, the structural variation of the resonator brings about the de-tuning of the resonance

Table 1. Dependence of fitted parameters γ_1, γ_2, κ, δ_1, and δ_2 on displacement distance (S). All the data are corresponded to that of Figure 4d and fitted using calculation (8).

S [μm]	γ_1 [rad ps^{-1}]	γ_2 [rad ps^{-1}]	κ [rad^2 ps^{-2}]	δ_1 [THz]	δ_2 [THz]
0	0.75	0.69	0.00	0	0
3	0.75	0.69	5.40	−0.008	0.013
4	0.75	0.69	8.72	−0.012	0.021
6	0.75	0.69	11.94	−0.018	0.031

frequency to the bright and dark modes, as indicated respectively by parameters δ_1 and δ_2 in Table 1 and Figure 6b. The fitted transmission spectra corresponding to $<\delta_1 = 0\,THz$, $\delta_2 = 0\,THz>$ and $<\delta_1 = 0.018\,THz$, $\delta_2 = 0.031\,THz>$ for $S = 6\,\mu m$, are reproduced in Figure 6c,d, respectively. After comparison, we conclude here that the main role of parameters δ_1 and δ_2 is to tune the transmission amplitude, thereby having little effect on the low-frequency (v_l) or high-frequency (v_h) shift. Further, the results depicted in Figure 6d demonstrate that the coupling coefficient (κ) can affect the shift of v_l and v_h and the transmission amplitude of the transparency peak resonance (v_t), indicating that it determines the transparency peak generation and the related oscillation resonance splitting near the resonance dip (i.e., the EIT effect).
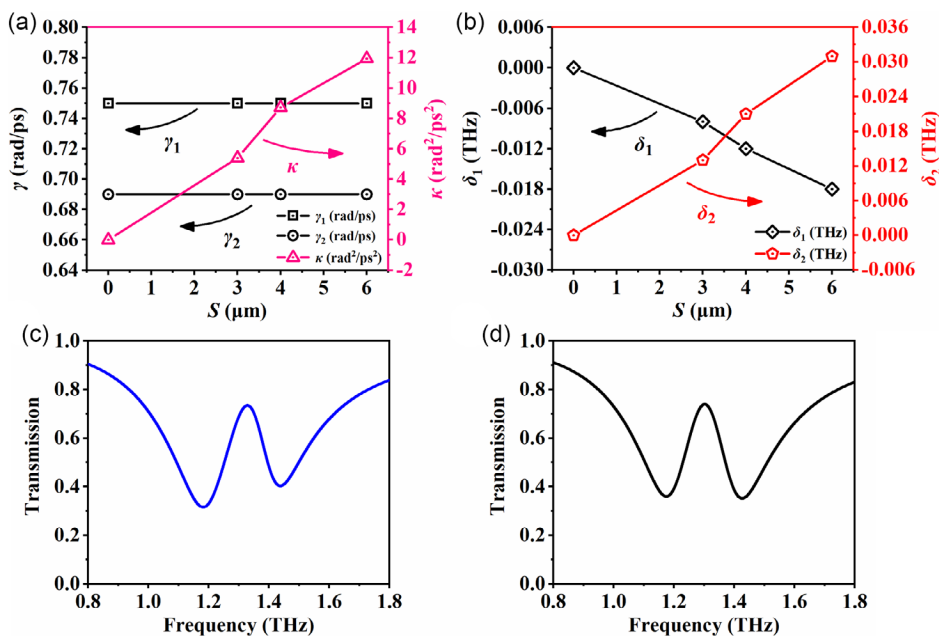
Figure 6. a,b) Dependence of the theoretically fitted parameters γ_1, γ_2, κ, δ_1, and δ_2 on the displacement distance (S). Fitted transmission spectra pertaining to the cases of c) $<\delta_1 = 0.018\,\text{THz}, \delta_2 = 0.031\,\text{THz}>$ and d) $<\delta_1 = 0\,\text{THz}, \delta_2 = 0\,\text{THz}>$, where the S value in the two graphs is 6 μm.

With the aforementioned deduction, analysis, and interpretation, as well as the viewpoints concerning the excitation of dark plasmonic modes in the symmetry-broken THz metamaterials as reported by Chowdhury et al.,[29] it becomes possible to account for the transmission spectral characteristics depicted in Figures 2 and 3. Metamaterials with high symmetry, as exemplarily reported in ref. [29], contain the dark plasmonic resonance modes that weakly interact with a certain linear-polarized electric field but can be aroused when breaking the structural symmetry of the designed resonators. In this concern, we postulate that the dark mode of the symmetric T-shaped resonator in this work is from the resonance excited by Y-polarized electric field, while the resonance excited directly by an incident THz field with X-polarization serves as the bright mode. In this frame, we associate the bright and dark modes in Figure 2 to the resonance dips at 1.39 THz and that at ≈1.0 THz, respectively. It also comes that the bright resonance is, logically, only measured at 1.39 THz in the symmetric T-shaped resonators while the dark resonance at ≈1.0 THz appears only after breaking the structural symmetry of the unit cell (Figure 2b). When the samples are clockwise rotated 90°, the resonance frequencies of the bright and dark modes are reversed accordingly, thereby leading to a single bright resonance at 1.0 THz in the symmetric resonator and an asymmetry-induced dark resonance at ≈1.39 THz (Figure 2d). All in all, the measured resonances are reversely consistent with each other, but they agree well with the bright and dark modes we postulated and anticipated.

4. Conclusion and Perspectives

To sum up, we have experimentally and theoretically investigated the variable electromagnetic responses of a THz metasurface by introducing a structural asymmetry to T-shaped resonators.

Based on the spectral characteristics collected in the experiments and theoretically stimulated, we have determined that the bright and dark modes in the T-shaped resonators are associated with the resonances excited respectively by X- and Y-polarized THz fields. Additionally, the coupled theory confirms the existence of the dark mode in the T-shaped resonators and, at the same time, reveals that the excitation of the dark mode, which can also be supported by the simulated EIT effect, is closely related to the enhanced coupling strength between the bright and dark modes subjected to the structural symmetry breaking. Moreover, although metasurface with changeable unit structure has been widely reported by a number of previous works for mimicking the quantum phenomenon of the EIT effect, simulating the experimentally observed symmetry-breaking-caused EIT effect in metasurface and explaining it from a theoretical point of view are still lacking at the current stage, needing a further exploration. Thus, our work not only presents a new theoretical understanding on the resonant modes in THz metamaterials with structural asymmetry breaking, but can also provide new insights into designing the optical devices based on asymmetric planar metasurfaces associated with controllable EIT and/or broadband transparency characteristics, including among others like broadband optical communication and/or filters, biological sensing and detection, and optical THz sensing, etc.

Conflict of Interest

The authors declare no conflict of interest.

Data Availability Statement

The data that support the findings of this study are available from the corresponding author upon reasonable request.

Keywords

[1] J. P. Marangos, *J. Mod. Opt.* **1998**, *45*, 471.

[2] M. Fleischhauer, A. Imamoglu, J. P. Marangos, *Rev. Mod. Phys.* **2005**, *77*, 633.

[3] C. Liu, Z. Dutton, C. H. Behroozi, L. V. Hau, *Nature* **2001**, *409*, 490.

[4] N. Yu, P. Genevet, M. A. Kats, F. Aieta, J.-P. Tetienne, F. Capasso, Z. Gaburro, *Science* **2011**, *334*, 333.

[5] A. Hatef, S. M. Sadeghi, M. R. Singh, *Nanotechonology* **2012**, *23*, 065701.

[6] C. Zhang, J. Wu, B. Jin, X. Jia, L. Kang, W. Xu, H. Wang, J. Chen, M. Tonouchi, P. Wu, *Appl. Phys. Lett.* **2017**, *110*, 241105.

[7] W. Li, D. Viscor, S. Hofferberth, I. Lesanovsky, *Phys. Rev. Lett.* **2014**, *112*, 243601.

[8] M. Mücke, E. Figueroa, J. Bochmann, C. Hahn, K. Murr, S. Ritter, C. J. Villas-Boas, G. Rempe, *Nature* **2010**, *465*, 755.

[9] H. Ahmad Khan, S. W. Shah, A. D. Khan, *Plasmonics* **2022**, *17*, 51.

[10] A. Naweed, G. Farca, S. I. Shopova, A. T. Rosenberger, in Frontiers in Optics, Optica Publishing Group, Tucson, Arizona, United States **2003**, p. MH6, https://opg.optica.org/abstract.cfm?uri=FiO-2003-MT71.

[11] C. Dong, V. Fiore, M. C. Kuzyk, H. Wang, *Science* **2012**, *338*, 1609.

[12] F. Xia, L. Sekaric, Y. Vlasov, *Nat. Photonics* **2007**, *1*, 65.

[13] Z. Zhang, J. Yang, X. He, Y. Han, J. Zhang, J. Huang, D. Chen, S. Xu, *Opt. Commun.* **2018**, *425*, 196.

[14] Z.-G. Dong, H. Liu, J.-X. Cao, T. Li, S.-M. Wang, S.-N. Zhu, X. Zhang, *Appl. Phys. Lett.* **2010**, *97*, 114101.

[15] C. Monat, M. de Sterke, B. J. Eggleton, *J. Opt.* **2010**, *12*, 104003.

[16] M. Manjappa, S. Y. Chiam, L. Q. Cong, A. A. Bettiol, W. L. Zhang, R. Singh, *Appl. Phys. Lett.* **2015**, *106*, 181101.

[17] R.-M. Ma, R. F. Oulton, V. J. Sorger, X. Zhang, *Laser Photonics Rev.* **2013**, *7*, 1.

[18] M. Baur, S. Filipp, R. Bianchetti, J. M. Fink, M. Goppl, L. Steffen, P. J. Leek, A. Blais, A. Wallraff, *Phys. Rev. Lett.* **2009**, *102*, 243602.

[19] D. R. Albert, D. L. Proctor, H. F. Davis, *Rev. Sci. Instrum.* **2013**, *84*, 063104.

[20] J. J. Longdell, E. Fraval, M. J. Sellars, N. B. Manson, *Phys. Rev. Lett.* **2005**, *95*, 063601.

[21] S. Zhang, D. Genov, Y. Wang, M. Liu, X. Zhang, *Phys. Rev. Lett.* **2008**, *101*, 047401.

[22] N. Liu, S. Kaiser, H. Giessen, *Adv. Mater.* **2008**, *20*, 4521.

[23] J. Gu, R. Singh, X. Liu, X. Zhang, Y. Ma, S. Zhang, S. A. Maier, Z. Tian, A. K. Azad, H. T. Chen, A. J. Taylor, J. Han, W. Zhang, *Nat. Commun.* **2012**, *3*, 1151.

[24] X. Su, C. Ouyang, N. Xu, S. Tan, J. Gu, Z. Tian, J. Han, F. Yan, W. Zhang, *IEEE Photonics J.* **2015**, *7*, 5900108.

[25] K. Zhang, C. Wang, L. Qin, R. W. Peng, D. H. Xu, X. Xiong, M. Wang, *Opt. Lett.* **2014**, *39*, 3539.

[26] X. Su, C. Ouyang, N. Xu, S. Tan, J. Gu, Z. Tian, R. Singh, S. Zhang, F. Yan, J. Han, W. Zhang, *Sci. Rep.* **2015**, *5*, 10823.

[27] S. Han, H. L. Yang, L. Y. Guo, *J. Appl. Phys.* **2013**, *114*, 163507.

[28] J. A. Burrow, R. Yahiaoui, A. Sarangan, I. Agha, J. Mathews, T. A. Searles, *Opt. Express* **2017**, *25*, 32540.

[29] D. R. Chowdhury, X. F. Su, Y. Zeng, X. S. Chen, A. J. Taylor, A. Azad, *Opt. Express* **2014**, *22*, 19401.

[30] P. Pitchappa, M. Manjappa, C. P. Ho, R. Singh, N. Singh, C. K. Lee, *Adv. Opt. Mater.* **2016**, *4*, 541.

[31] R. Yahiaoui, J. A. Burrow, S. M. Mekonen, A. Sarangan, J. Mathews, I. Agha, T. Searles, *Phys. Rev. B* **2018**, *97*, 155403.

[32] R. Singh, I. A. I. Al-Naib, Y. P. Yang, D. R. Chowdhury, W. Cao, C. Rockstuhl, T. Ozaki, R. Morandotti, W. Zhang, *Appl. Phys. Lett.* **2011**, *99*, 201107.

[33] Y. Srivastava, M. Manjappa, L. Cong, W. Cao, I. Al-Naib, W. Zhang, R. Singh, *Adv. Opt. Mater.* **2016**, *4*, 457.

[34] C. Chen, I. Un, N. Tai, T. Yen, *Opt. Express* **2009**, *17*, 15372.

[35] F. Cheng, X. Yang, J. Gao, *Sci. Rep.* **2015**, *5*, 14327.

[36] R. Singh, W. Cao, I. Al-Naib, L. Cong, W. Withayachumnankul, W. Zhang, *Appl. Phys. Lett.* **2014**, *105*, 171101.

[37] I. Vendik, O. Vendik, *Tech. Phys.* **2013**, *58*, 1.

[38] W. Yang, Y.-S. Lin, *Opt. Express* **2020**, *28*, 17620.

[39] J. Federici, L. Moeller, *J. Appl. Phys.* **2020**, *107*, 111101.

[40] T. D. Gupta, L. Martin-Monier, W. Yan, A. L. Bris, T. Nguyen-Dang, A. G. Page, K.-T. Ho, F. Yesilköy, H. Altug, Y. P. Qu, F. Sorin, *Nat. Nanotechnol.* **2019**, *14*, 320.

[41] L. Q. Liu, X. H. Zhang, Z. Y. Zhao, M. B. Pu, P. Gao, Y. F. Luo, J. J. Jin, C. T. Wang, X. G. Luo, *Adv. Opt. Mater.* **2016**, *5*, 1700429.

[42] L. Q. Cong, W. Cao, X. Q. Zhang, Z. Tian, J. Q. Gu, R. J. Singh, J. G. Han, W. L. Zhang, *Appl. Phys. Lett.* **2013**, *103*, 171107.

[43] N. Savvides, H. J. Goldsmid, *J. Phys. C: Solid State Phys.* **1973**, *6*, 1701.

[44] M. Mehnaj, C. N. Ahmed, *Int. J. Eng. Res.* **2014**, *3*, 584.

[45] X. Q. Su, C. M. Ouyang, N. N. Xu, S. Y. Tan, J. Q. Gu, Z. Tian, J. G. Han, F. P. Yan, W. L. Zhang, *IEEE Photonics J.* **2015**, *7*, 5900108.

[46] X. Q. Su, C. M. Ouyang, N. N. Xu, S. Y. Tan, J. Q. Gu, Z. Tian, R. Singh, S. Zhang, F. P. Yan, J. G. Han, W. L. Zhang, *Sci. Rep.* **2015**, *5*, 10823.